

Band structure, band offsets, substitutional doping, and Schottky barriers of bulk and monolayer InSe

Yuzheng Guo^{1,2} and John Robertson¹

¹*Department of Engineering, Cambridge University, Cambridge CB2 1PZ, United Kingdom*

²*College of Engineering, Swansea University, Swansea SA1 8EN, United Kingdom*

(Received 19 May 2017; published 11 September 2017)

We present a detailed study of the electronic structure of the layered semiconductor InSe. We calculate the band structure of the monolayer and bulk material using density functional theory, hybrid functionals, and *GW*. The band gap of the monolayer InSe is calculated to be 2.4 eV in screened exchange hybrid functional, close to the experimental photoluminescence gap. The electron affinities and band offsets are calculated for vertical stacked-layer heterostructures, and are found to be suitable for tunnel field effect transistors (TFETs) in combination with WSe₂ or similar. The valence-band edge of InSe is calculated to lie 5.2 eV below the vacuum level, similar to that for the closed shell systems HfSe₂ or SnSe₂. Hence InSe would be suitable to act as a *p*-type drain in the TFET. The intrinsic defects are calculated. For Se-rich layers, the Se adatom (interstitial) is found to be the most stable defect, whereas for In-rich layers, the Se vacancy is the most stable for the neutral state. Antisites tend to have energies just above those of vacancies. The Se antisite distorts towards a bond-breaking distortion as in the EL2 center of GaAs. Both substitutional donors and acceptors are calculated to be shallow, and effective dopants. They do not reconstruct to form nondoping configurations as occurs in black phosphorus. Finally, the Schottky barriers of metals on InSe are found to be strongly pinned by metal induced gap states (MIGS) at ~ 0.5 eV above the valence-band edge. Any interfacial defects would lead to a stronger pinning at a similar energy. Overall, InSe is an effective semiconductor combining the good features of 2D (lack of dangling bonds, etc.) with the good features of 3D (effective doping), which few others achieve.

DOI: [10.1103/PhysRevMaterials.1.044004](https://doi.org/10.1103/PhysRevMaterials.1.044004)

I. INTRODUCTION

There is presently considerable interest in the layered materials such as the transition metal dichalcogenides (TMDs) and graphene. Graphene is a zero-band-gap semimetal with an extremely high carrier mobility. However, the absence of a band gap makes it of minor interest for field effect transistors needing power gain [1]. TMDs are true 2D semiconductors with a band gap [2]. However, their carrier mobilities are typically only of order $100 \text{ cm}^2 \text{ V}^{-1} \text{ s}^{-1}$, [3] much less than those of graphene, as their band edge states have *d*-like character. An advantage of TMDs is that there is a wide range of them with different band gaps and electron affinities [4,5], so that they could be used in heterostructures in devices such as tunnel field effect transistors.

Black phosphorus (b-P) is another 2D semiconductor with a band gap, and its carrier mobility of $\sim 1000 \text{ cm}^2 \text{ V}^{-1} \text{ s}^{-1}$ is much higher than that of TMDs because b-P has band edges that are *p*-like in character [6]. However, b-P reacts with water so its devices must be encapsulated. Also, its open, flexible lattice allows many substitutional dopants to reconstruct into distorted, nondoping configurations rather than act as shallow substitutional donors or acceptors [7]. Thus, despite its high carrier mobilities, b-P is not a very practical semiconductor.

There is a third class of 2D semiconductors, the GaSe and InSe family [8–11]. These consist of a vertically stacked metal-chalcogen double layers with covalent bonding within the layers and van der Waals bonding between the layers. Carrier mobilities in InSe are of order $1000\text{--}2000 \text{ cm}^2 \text{ V}^{-1} \text{ s}^{-1}$ [10,11], similar to those of black phosphorus as they also have *s*, *p*-like band edge states. Recently, the quantum Hall effect was observed in the two-dimensional electron gas in InSe few-layer films [10]. Thus it is important to

understand the electronic structure of InSe, including its band offsets and dopant properties relevant to its use in electronic devices. A device of particular interest is the tunnel field effect transistor (TFET) [12], which is a leading candidate for steep slope (low-power) transistors [12]. TFETs need a semiconductor heterojunction with a type-II (staggered) or type-III (broken gap) band offset. They are typically made from III-V semiconductors, but the lattice matching condition needed for this introduces many interfacial defects, which can limit performance [13]. TFETs made from stacked layers of two-dimensional semiconductors do not require lattice matching, and so in principle they do not suffer from this type of defect. InSe could be used in such a device with another 2D semiconductor such as WSe₂. A final point is that TMD devices tend to be limited by their contact resistances [14,15]. Thus we also study the Schottky barrier heights of various metals on InSe semiconductors using explicit supercell calculations.

II. METHODS

The calculations are carried out using the plane-wave density-functional code CASTEP [16]. Norm-conserving pseudopotentials are used with a cutoff energy of 500 eV. The In pseudopotential includes the shallow In *4d* core levels in the valence shell. Grimme's method [17] is used to correct the density functional theory (DFT) treatment of the van der Waals interactions. The standard DFT method underestimates the band gap of semiconductors and insulators. Thus we use the screened exchange (sX) hybrid density functional [18] to correct these band gap errors. Hybrid functionals such as sX and HSE have been previously applied to the electronic and defect calculations in other 2D systems such as MoS₂ [19–21].

The sX includes 100% HF exchange, and we use the standard Thomas-Fermi screening length [18] evaluated for the valence electron density of bulk InSe, $k_s = 2.01 \text{ \AA}^{-1}$.

Similar parameters were used as in the CASTEP density functional calculations to give the Kohn-Sham orbitals. A $4 \times 4 \times 4$ k -point mesh is used for the G_0W_0 calculation based on the Kohn-Sham orbitals. 214 empty states are included in the calculation for the primitive cell to give an energy convergence to less than 0.03 eV.

For mono- and few-layer systems, the screening is significantly lower, and the exciton binding energy becomes large. The quasiparticle band gap becomes larger than the optical band gap. For this case, we use the GW method to calculate the quasiparticle band gap. G_0W_0 calculations were performed with the Quantum Espresso code using norm-conserving pseudopotentials and an energy cutoff of 70 Ry.

We use a supercell model for the mono- and few-layer systems, with a vacuum layer of 25 Å between the layer blocks. This is checked to be a good approximation for a 2D slab system. The defect calculations used 120-atom supercells for the few-layer and bulk cases. The minimum distance between mirror image defects is 22 Å. A $2 \times 2 \times 2$ Monkhorst-Pack k -point mesh is used for reciprocal space integration in all supercells. The above parameters lead to an energy convergence of less than 0.01 eV. The density of states calculations use a k -point mesh of $9 \times 9 \times 1$.

For defects, the charge transition states are calculated using the supercell method. Corrections for defect charges and band occupations are applied as in Lany and Zunger's scheme [22]. The total energy of the perfect supercell (E_H) and the supercell with defect (E_q) are calculated for different charge states. The defect formation energy H_q is then found from

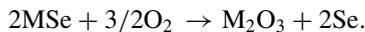
$$H_q(E_F) = [E_q - E_H] + q(E_v + \Delta E_F), \quad (1)$$

where qE_v is the change in Fermi energy when charge q is added. No extra correction is needed for a two-dimensional calculation.

III. RESULTS AND DISCUSSION

A. Environmental stability

At present, InSe seems to be preferred over GaSe for experimental studies of semiconductor transport. This has arisen because InSe is more environmentally stable against oxidation in damp conditions than GaSe [23,24]. We can see this by comparing the heat of reaction for oxidation,



Using the experimental heat of formation of bulk GaSe and InSe, we find that the oxidation reaction of GaSe is exothermic by 3.85 eV per GaSe formula unit whereas the oxidation of reaction of InSe is exothermic by 3.49 eV per formula unit. This accounts for the reduced environmental stability of GaSe [22] compared to InSe.

B. Band structures

Figure 1(a,inset) shows the atomic structure of InSe. It consists of four atomic layers in which In occupies fourfold coordinated sites with In-In bonds, and Se occupies threefold

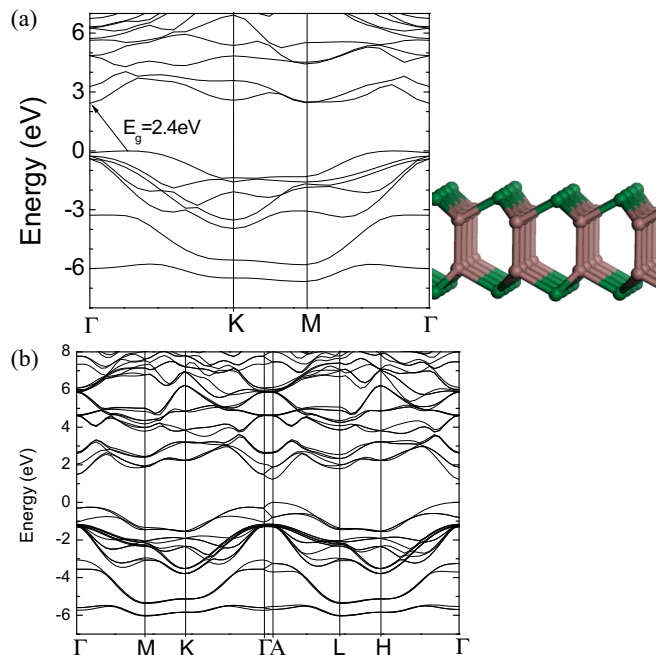


FIG. 1. Band structures of (a) monolayer and (b) bulk InSe calculated using the screened exchange functional. The conventional unit cell is used for bulk. Inset, structure of an InSe monolayer (green = Se, brown = In).

coordinated sites on the outside of the layers with van der Waals bonding between layers. GaSe and GaS bulk adopt the β -GaSe or 2H structure. On the other hand, bulk InSe tends to adopt the γ or 3R structure. We set all these III-VI compounds into the 2H structure for ease of comparison.

Figures 1(a) and 1(b) show the band structure of an InSe monolayer and bulk using the sX functional. The basic ordering of bands is similar to that found by others [25–32]. The lowest lying Se 4s states are omitted from the figure. The In 4d states lie at 16 eV, and are also off the bottom of the figure. Unlike MLMoS₂, the band gap of ML InSe is indirect. The minimum of the conduction band lies at Γ , and the valence-band maximum lies just away from Γ in the ΓK direction. This leads to the inverted “Mexican-hat” valence-band structure that has been noted by others [29,31].

Table I compares the minimum band gaps of the four MX semiconductors in the generalized gradient approximation (GGA), sX, and G_0W_0 approximations. Our GW values are similar to those found by others [30,33–35]. Table II gives the calculated band gaps of InSe as a function of the number of

TABLE I. Minimum band gaps (eV) of the III-VI chalcogenides.

monolayer	GaS	GaSe	InS	InSe
GGA	1.63	1.51	1.54	1.44
sX	2.72	2.53	2.58	2.41
GW	3.82	3.64	3.13	2.87
bulk	GaS	GaSe	InS	InSe
GGA	0.57	0.51	0.52	0.49
sX	1.59	1.48	1.46	1.25

TABLE II. Calculated band gaps (eV) of InSe, from GGA and sX methods vs number of layers. Also shown is the experimental exciton (optical) band gap [10].

number of layers	1	2	3	4	5	bulk
GGA	1.44	0.97	0.81	0.73	0.68	0.49
sX	2.40	1.90	1.73	1.65	1.60	1.40
Optical gap (exp) [10]	2.92	1.89	1.77	1.56	1.47	1.25

layers, in GGA, and then sX. As in black phosphorus [7], the gap E_g depends on the number of layers N according to

$$E_g(N) = E_b + (E_1 - E_b)/N, \quad (2)$$

where E_1 is the gap of the monolayer and E_b is the gap of the bulk.

Table III gives the calculated effective band masses for InSe. The in-plane effective electron mass m_{\parallel}^e of $0.23 m_0$ at Γ is similar to those of other authors [36–39]. The in-plane hole mass m_{\parallel}^h at Γ is very high because of the Mexican hat property. This is the source of the mass anisotropic reversal noted many years ago [39]. The electron mass at the K point is larger than at Γ .

Some comments might be useful on the band gaps. In three-dimensionally bonded semiconductors or bulk two-dimensional semiconductors, the exciton binding energy is small, and the GW and the hybrid functionals HSE and SX all give the quasiparticle (QP) band gap. For few layer 2D materials, the screening becomes weaker, and the QP band gap increases considerably. The GW method still describes this correctly. However, the sX and HSE methods as presently parameterized do not include this reduced screening, and so their band gaps do not follow the GW gap upwards. The optical or exciton band gap is given by the QP gap minus the exciton binding energy. Thus, by an accidental cancellation of errors, the HSE and sX band gaps tend to follow the optical band gaps for the few layer situation, which can be seen in Table I. This was noticed previously for MoS₂ by Scuseria [40].

C. Band character

Each of the bands of GaSe or InSe is known to have a specific atomic and orbital character, as was noted by Schluter [27] from an analysis of charge densities from pseudopotential calculations, by Robertson [28] from tight-binding theory, and recently by Zolyomi [29]. The main peak of the valence-band density of states consists of Se $p_{x,y}$ states in a bonding

combination with In $p_{x,y}$ states. Below this lies a pair of bands at -3 to -6 eV in which In s states interact with Se p_z states. These states are bonding along both the In-Se bond and the In-In bond. The bands forming the valence-band top and the conduction-band bottom each consist of In s and Se p_z states. The VB top has antibonding character along the In-Se bond and bonding character along the In-In bond, whereas the CB bottom is antibonding along the In-Se bond and along the In-In bond. Thus the minimum band gap has a bonding to antibonding transition across the In-In bond. This is consistent with the In and Se valences. The Se $4s$ states are fully occupied. The In and Se $p_{x,y}$ states are half-filled overall. The In $5s$ states are half-filled and the Se p_z states are filled, by filling only the bonding combination along the In-In bond.

This partial bonding character of the bands near the gap explains why the band gaps of the GaSe-InSe series vary much less by the replacement of Ga by In than for the equivalent InGaAs alloys. For example, the band gap shrinks from 1.45 to 0.33 eV for the GaAs to InAs compounds because this is dominated by the lowering of the atomic s state from Ga to In, whereas the gap of GaSe to InSe compounds depends on the much smaller reduction of the gap of the Ga-Ga bond to the In-In bond. It is also relevant that the calculated Bader charges for In and Se are $+0.15e$ and $-0.15e$, which shows that the metal-chalcogen bonding is not very polar.

D. Band edge energies and band offsets

We have previously calculated the energies of the valence-band maximum (VBM) and conduction-band minimum (CBM) of the monochalcogenides with respect to the vacuum level using a supercell model. The energy of the VBM is called the ionization potential (IP) and that of the CBM is called to electron affinity (EA). A 25-Å vacuum gap is left between the InSe layers. The electrostatic potential is then calculated for each layer normal to the layers, averaged along these layers. The potential within the vacuum gap denotes the vacuum potential. The IP and EA can then be determined with respect to this potential. It is well known that the GGA underestimates semiconductor band gaps, and that hybrid functionals can be used to correct this error [18]. It is less known that the GGA also makes errors in the IP, and hybrid functionals can also correct this error [41]. Sometimes, the amount of exchange mixed into the hybrid functional is varied to fit the band gap [42–44]. It should be noted that a functional and a potential that give a correct band gap do not necessarily give the correct IP; this must be tested [42].

In particular, it is advisable to use pseudopotentials that retain the shallow cation d core levels in the valence shell in order to get the correct gap and IP together. A particular problem occurs in compounds such as ZnO with shallow cation semicore d states [43]. For these oxides, including ZnO, In₂O₃, and SnO₂, GGA grossly underestimates the band gap. A hybrid functional will correct some of this error but not all. Then, some groups increase the fraction of HF exchange to fit the gap. However, there are two GGA errors for ZnO, the normal GGA underestimation of the gap, and secondly that the Zn $3d$ states are still too high, so they are still repelling the VBM upwards. It is first necessary to ensure the Zn $3d$ states are low enough before fitting the gap, otherwise there is an asymmetric

TABLE III. Calculated effective masses, parallel or perpendicular to the layers.

	mass
m_{\parallel}^e	0.23
m_{\parallel}^h	3.9
$m_{\parallel c}^h$	0.17
m_{\parallel}^e (at K point)	0.5
$m_{\parallel c}^h$ (at K point)	0.18

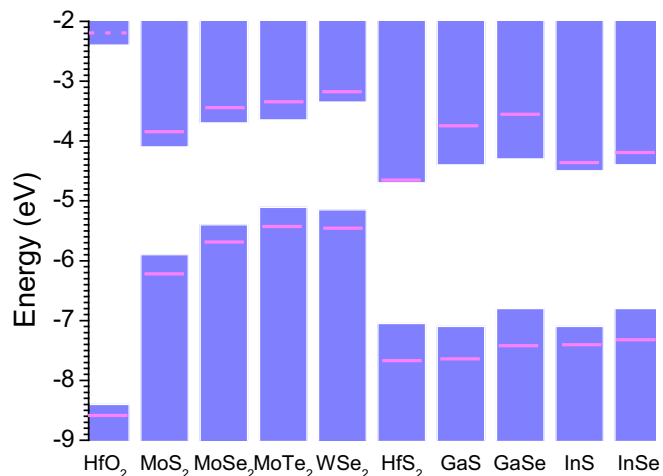


FIG. 2. The band alignment of InSe, various other 2D semiconductors and a gate insulator HfO_2 , for the stacked layer configuration where the electron affinity rule holds [45]. The band edges are aligned against the vacuum level. The band energies are those given by screened exchange (sX). The dashed pink lines are the GW band energies (see text).

error. This occurs in HSE but not in sX. InSe belongs to this class of compounds due to its shallow In $4d$ states.

Figure 2 shows the VBM and CBM energies calculated using the sX functional, referenced to the vacuum level. They are plotted together with the band energies of some TMDs and of HfS_2 [45]. GW energies are included for completeness [5]. We see that the band edges of the GaSe series lie close to those of HfS_2 , whereas the MoS_2 series lie higher in energy. This follows from HfS_2 being a closed shell d^0 semiconductor, whereas WSe_2 or MoS_2 have a d^2 configuration with a partly filled d band, which raises the E_F by one band towards the vacuum level.

A tunnel FET requires a type-II (staggered) or type-III (broken) band alignment, in which the conduction-band edge of semiconductor A is level with the valence-band edge of semiconductor B. This will cut off the high-energy tail of the electron energy distribution and so achieve a small subthreshold slope, below the thermal limit of e/kT or 60 mV/decade, where e is the electronic charge. This can be done using two III-V semiconductors, but this would require a lattice matching of the two semiconductors. The advantage of a stacked vdW heterojunction is that the two semiconductors can be chosen solely in terms of their band gaps and band offsets, as the lattice matching is not necessary because the weak van der Waals bonding does not create defects. Band offsets in the stacked configuration follow the electron affinity rule. It was previously noted that WSe_2 with HfS_2 or SnS_2 would be a suitable choice for a TFET heterojunction, because the CBM of HfS_2 or SnS_2 aligns with the VBM of WSe_2 [4,45]. However, the acceptor states in HfS_2 are not particularly shallow, and HfS_2 does not have a high hole mobility, whereas SnS_2 has good electronic properties [46] but its phase stability region might be too small for CVD conditions [47].

We see from the band alignments in Fig. 2 that InSe is suitable as a component of a TFET heterojunction. Its band gap is reasonable, its CBM is quite deep below the

TABLE IV. Defect formation energy in their neutral state. Lowest value in bold.

Se-rich limit	eV
Se_i	1.32
Se_{In}	1.2
V_{In}	4.0
In-rich limit	
In_i	1.9
In_{Se}	1.65
V_{Se}	1.05

vacuum level, giving it a type-II alignment against WSe_2 . However, its CBM is not quite low enough to show a type II/III alignment which would be more desirable. Nevertheless, overall, comparing mobility, synthesis, dopant behavior and band alignment, then InSe is so far the favorable choice for use in TFET heterojunctions.

Figure 2 also shows the alignment of HfO_2 , which would be a typical gate oxide used in the TFET. We see that the band offsets of both valence and conduction bands of HfO_2 to InSe are over 1 eV, so that HfO_2 will limit current injection into both bands.

E. Intrinsic defects

We have also calculated the defect states and formation energies of various intrinsic defects in InSe. The formation energies are calculated as a function of the Fermi energy E_F , following Eq. (1). Correction factors must be applied in terms of the band occupations and the charged defects. This is done following the method of Lany and Zunger [22]. Table IV gives a summary of the defect formation energies in their neutral configuration.

Figure 3(a) shows a Se adatom, equivalent to a Se interstitial, lying on top of another Se. This is the most stable defect for the Se-rich condition. The neutral state has a defect formation energy of 1.23 eV. Figure 3(c) shows an In vacancy. Removing an In from the central In-In dimer allows the Se atoms on both sides to bond to the remaining In atom. The diamagnetic -1 state is the most stable for Fermi energies across most of the band gap, Fig. 3(d). The In then forms three sets of three-center bonds to its 6 neighbors.

Figure 3(e) shows the Se vacancy. This has an interesting relaxation in which the three surrounding In atoms move closer to each other and form In-In bonds. For the neutral case, the relaxation is symmetric, but for the -2 case, the relaxation is asymmetric, with two short bonds, and one long bond, almost unbonded, because this link is really two filled dangling bond states pointing at each other. Its charge states are similar to that of the Se vacancy in MoSe_2 [20]. Figure 3(g) shows the “In interstitial” or adatom. This adds on top of the Se-In-In-Se layer, in a hollow site of the Se layer below. It is equivalent to the Lewis base noted elsewhere. Overall, the Se vacancy is more stable than the In adatom for In-rich conditions. The In adatom is stable in the $+1$ state for most Fermi energy positions, because this is a diamagnetic state. It is interesting that substitutional donors and acceptors show little reconstruction of their bonding, as noted in the next section, while the native defects show an interesting combination of

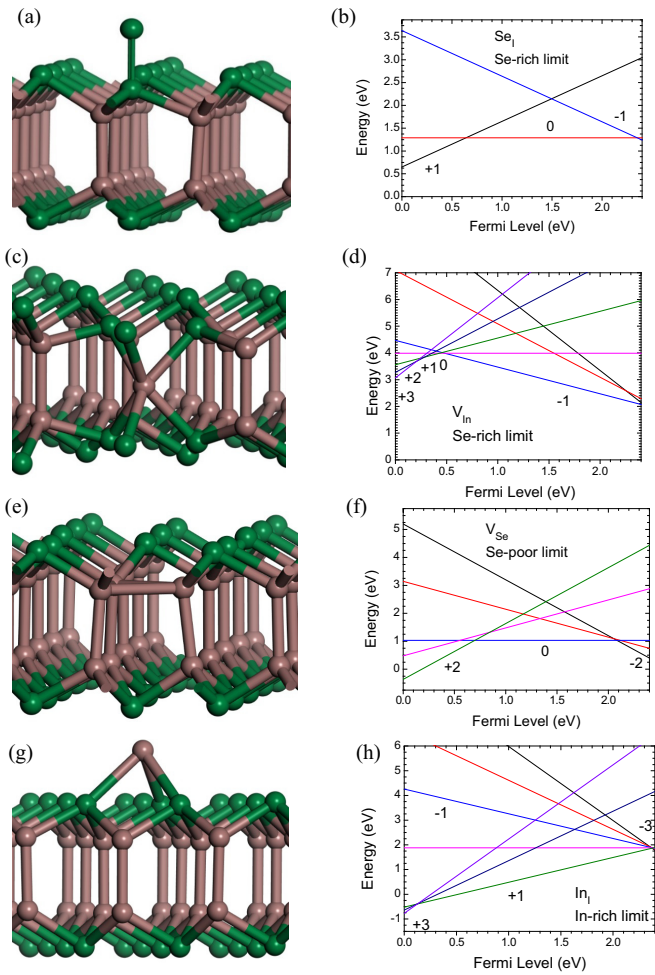


FIG. 3. Atomic structure of intrinsic defects. [(a) and (b)] Se adatom, [(c) and (d)] In vacancy, [(e) and (f)] Se vacancy, and [(g) and (h)] In interstitial.

minor reconstruction plus adatom behavior, which is possible because of their layered structure.

Figure 4 shows the properties of the antisites. The Se_{In} antisite is the most stable of the Se excess sites, being 0.1 eV more stable than the Se_i adatom in its neutral configuration. On the other hand, the In_{Se} antisite is only the second most stable of the In excess sites, being 0.6 eV less stable than the V_{Se} . Thus the overall defect properties of antisites versus vacancies are different in InSe from those of MoS_2 where the S vacancy is by far the most low cost defect [48,49].

Overall, the antisites of InSe have more in common with those of GaAs than those of MoS_2 . This is because In and Se are *s*, *p*-bonded elements, like Ga and As, whereas Mo and S are chemically quite different.

The Se_{In} antisite shown in Fig. 4(a) is distorted in its neutral configuration, with one longer Se-Se bond, and two shorter Se-Se bonds. Se has three more valence electrons than In, and these electrons try to fill up states of Se-Se bonds. This occurs by breaking a Se-Se bond and forming two Se dangling bonds (DBs), which can then take four electrons.

This geometry resembles that of the EL2 complex of GaAs [50,51], where the As_{Ga} antisite is moving off-center along

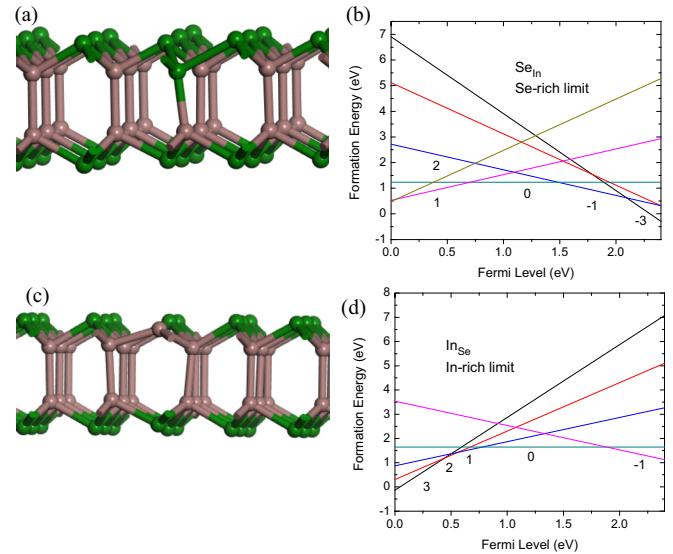


FIG. 4. [(a) and (b)] Geometry and defect formation energies vs Fermi energy for Se_{In} antisites. [(c) and (d)] Geometry and defect formation energies vs Fermi energy for In_{Se} antisites.

(111) to partially break an As-As bond and form a vacancy and an As interstitial.

Figure 4(b) shows the electronic transitions of the Se antisites in InSe. The neutral state has unpaired electrons and this makes the diamagnetic +1 and -1 states relatively more stable. The neutral state is the most stable for E_F between 0.6 and 1.5 eV, while the +1 and -1 states are more stable for most of the remaining energies in the gap.

Figure 4(c) shows the In_{Se} antisite geometry in its neutral state. Here, the In site has moved downwards and “flattened out.” This is because of the deficit of three electrons compared to the original lattice. This leads to this In site adopting a near planar “*s p*²-like” bond configuration with an empty π state perpendicular to the bonding plane.

Figure 4(d) shows the transition levels. The neutral configuration is stable for E_F between 0.7 and 1.8 eV, and then the -3 and +1 diamagnetic states are more stable at the ends. The transition energies of this antisite are broadly similar to those of the Se vacancy, so that these defects would have broadly similar pinning energies if they were created at metal-InSe contacts, see later.

F. Substitutional dopants

The *n*-type dopants are group VII elements at the Se site or group IV elements at the In site. The expected acceptors are group V elements at the Se site, and group II elements at the In site. The doping electrical levels are summarized in Fig. 5.

Figure 6(a) shows the relaxed geometry of the neutral substitutional Br donor at the Se site. There is very little lattice relaxation for this defect compared to the undoped lattice. Figure 6(b) shows the formation energy of Br_{Se} as a function of E_F . It shows that the +/0 transition lies at 150 mV below the CBM. This is reasonably shallow. It is consistent with the experimentally observed shallowness of donors in bulk InSe.

Figure 6(c) shows the relaxed structure of the substitutional P acceptors at the Se site. It also shows that there is little

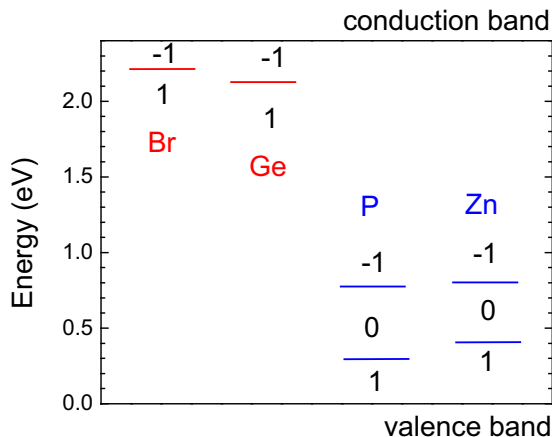


FIG. 5. The doping defect levels in the band gap. Br and Ge are *n* type. P and Zn are *p* type.

distortion compared to the undoped lattice. Figure 5(d) shows the defect formation energy versus E_F , and the donor transition at an energy of 550 mV above the VBM, a moderately deep acceptor.

Figure 6(e) shows the substitutional Ge donor at the In site. There is no lattice relaxation. The +1/0 transition is

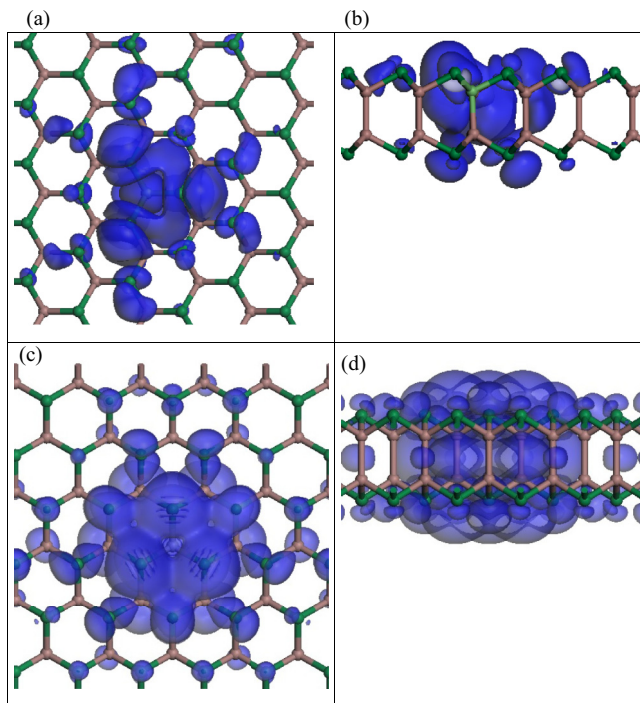


FIG. 7. [(a) and (b)] Donor state wave function for substitutional Ge at In site, top and side view. [(c) and (d)] Acceptor state wave function for substitutional Zn at In site, top and side view.

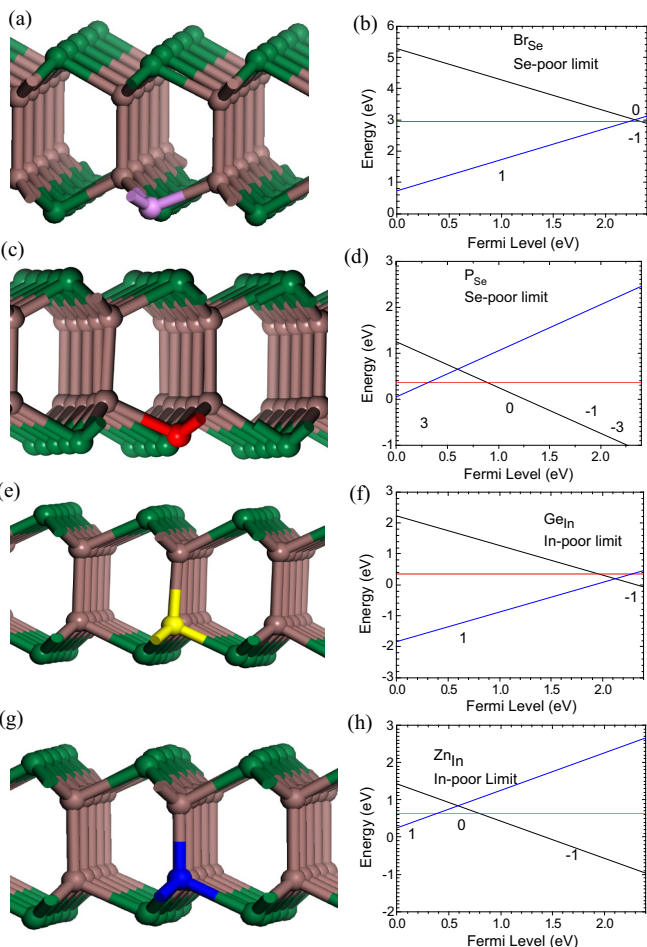


FIG. 6. Atomic structure and defect transition level of various dopants in InSe. [(a) and (b)] Br: pink, [(c) and (d)] P: red, [(e) and (f)] Ge: yellow, and [(g) and (h)] Zn: blue.

calculated to lie at 250 mV below the CBM in Fig. 6(f), and is borderline shallow. Figure 6(g) shows the structure of the substitutional Zn at the In site for the monolayer. The $-/0$ transition is calculated to lie at 550 mV above the VBM which is also relatively deep.

Both the donors and acceptors are known to be shallow in bulk InSe [37,38]. Figure 7 shows the calculated wave functions of the donor and acceptor states in monolayer InSe for a side view and top view. The in-plane Bohr radius of donors is $\sim 4 \text{ \AA}$, whereas for acceptors it is 6.5 \AA . The binding energies are a function of the dielectric constant and the effective masses. In the monolayers, the dielectric constant declines below the bulk value because of the lower screening. The effective masses of both holes and electrons are quite low in GaSe and surprisingly isotropic for the layered material [36,39]. Thus the binding energies are expected to increase above their bulk values, but remain quite shallow.

The key observation for the behavior of the substitutional dopants in InSe is that they remain in substitutional doping configurations. They do not undergo reconstructions like those in b-P, where the dopant sites distort to form nondoping sites obeying the 8-N rule bonding as in amorphous semiconductors [7,52]. Nor do dopants have the relatively deep character of some dopants in MoS₂ [53]. These factors are principally because the low effective masses lessen the defect state localization, which lessens the coupling to Jahn-Teller type distortions towards nondoping configurations. Thus InSe has the advantage that although it is formally a 2D semiconductor, its greater layer thickness and *sp* bonding gives it the lower effective band mass and shallow dopant characteristics of 3D semiconductors. On the other hand, it retains the advantage of

the no lattice-matching condition and low carrier scattering of a 2D semiconductor.

G. Contact properties

The performance of devices in 2D materials is often limited by their contact resistances [14,15]. In some cases, this is because the contacts have the “on-top” geometry, for others it is because of the presence of Schottky barriers. In general, the Schottky barrier heights are pinned to a certain degree, depending on the density of gap states at the interface, with greater pinning for more gap states [54–57]. These gap states can be the intrinsic “metal induced gap states” (MIGS) or by extrinsic states due to defects, depending on which is more numerous. The defects arise if there is a chemical reaction between the electrode metal and the semiconductor.

We first consider the case of intrinsic gap states at ideal (nondefective) interfaces, in the on-top or “stacked” geometry, following previous work on MoS₂ [58–60]. The calculations use supercells with a monolayer of InSe, and five layers of various metals in their FCC phase attached by their (111) faces onto InSe. A typical supercell is shown in Fig. 8(a). The InSe lattice is rotated if necessary to give a lattice matching to the overlying metal. This slab is separated by 25 Å of vacuum. The energy difference between the metal Fermi energy and the InSe VBM is then extracted from the partial density of states to define the p-type Schottky barrier height (SBH). There is often considerable hybridization between the InSe states and the metal, so that the InSe VBM energy can be difficult to identify in the combined system [35,48]. For this purpose, we use the In 4*d* core level as a reference energy to identify the VBM [48]. The *n*-type SBH ϕ_n from the CBM is then plotted versus the experimental work function of the contact metal [61] as in Fig. 8(b). We see that the data follow a linear relation, which can be expressed as [57]

$$\phi_n = E_{\text{cni}} - \chi + S(\Phi_M - E_{\text{cni}}), \quad (3)$$

where χ is the electron affinity of the semiconductor, Φ_M is the work function of the metal contact (both from the vacuum level), and S is the Schottky barrier pinning factor, given by $d\phi_n/d\Phi_M$. Within the metal induced gap state model of SBHs, E_{cni} is the semiconductor’s charge neutrality (CNL) reference energy (from the vacuum level) [55], the energy up to which the MIGS are occupied on a neutral surface.

The pinning factor extracted from Fig. 8(b) is $S = 0.18$. This relatively low value of S indicates that there is considerable Fermi level pinning by the MIGS. It means that it is not so easy to vary the metal work function to obtain an Ohmic contact. The MIGS model applies to this van der Waals solid, because the metal layers actually form bonds to the Se sites. This can be seen from the short bonding distances in Fig. 7(a).

The charge neutrality level is the reference level of the MIGS. It can be calculated from the density of states $N(E)$ as the energy at which the Greens function is zero [55],

$$G(E) = \int \frac{N(E')dE'}{E - E'} = 0. \quad (4)$$

Here we retain only the In and Se *s*, *p* valence states but exclude the In 4*d* core states, as the latter are too localized to interact strongly with the MIGS. This gives a CNL energy of

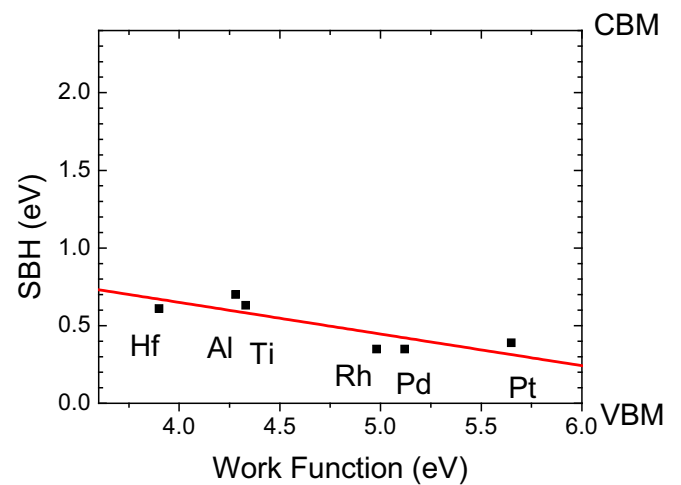
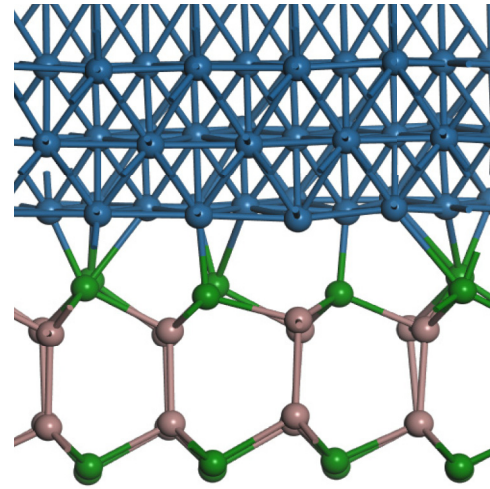


FIG. 8. (a) The supercell used to calculate the InSe/Pt Schottky barrier height. (b) Calculated barrier heights for various metal layers on monolayer InSe. The VBM is set to be 0 eV. The pinning factor S (slope of red line) is found to be 0.18.

0.58 eV (from the valence-band edge) for the isotropic case. This is very close to the energy when extracted from the fit of Eq. (3) to the data points in Fig. 7(b).

The value $S = 0.18$ for InSe compares with a value of $S = 0.28$ calculated for a defect-free MoS₂ layer [60]. It is interesting that our theoretical value $S = 0.18$ is also close to the old experimental value of Kurtin and Mead [62] of $S = 0.26$ for GaSe. (Note that their slope of barrier height versus Pauling electronegativity must be converted to the dimensionless barrier height versus electronegativity [63] by the conversion factor of 2.27.) It is also fairly close to the value calculated for the ideal barrier using Monch’s [56] dependence of S on optical dielectric constant, $S = 0.21$. This means that the experimental pinning factor for InSe is that for the defect-free interface. This contrasts with the behavior of MoS₂. In that case, the experimental pinning factor $S = 0.1$ [14] is much lower than the theoretical value of 0.3 for its ideal interface [60], and corresponds to pinning by defects [21]. The defects for InSe are expected to be chalcogen vacancies, formed by reaction with the contact metal [19,64]. These

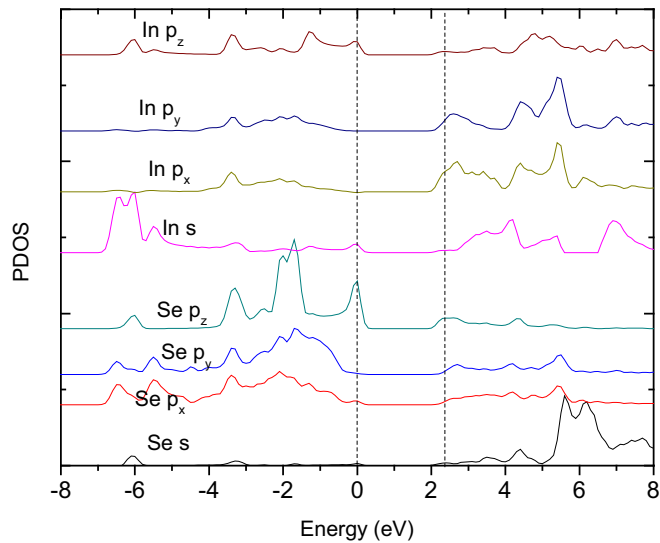


FIG. 9. Partial DOS of InSe decomposed into orbital symmetry.

would pin E_F at the $0/2+$ vacancy energy or at 0.7 eV above the VBM from Fig. 3. Given that the formation energy of chalcogen vacancies is similar for each compound (~ 1.0 eV in the S/Se poor limit) it is unclear why the contact formation process is chemically different in these two cases. On the other hand, there are different and interesting reports on the degree of chemical reaction of metals at GaSe contacts [65], which deserve further attention.

It was noted in MoS₂ that the CNL energy depended strongly on the orientation [60], with the CNL for stacked

contacts using the z oriented states being different to that for the lateral contacts, which use the x, y states of the in-plane bonds. To check this effect for InSe, we calculated the orbital resolved PDOS of InSe monolayers as shown in Fig. 9. Applying Eq. (4) to the $p_{x,y}$ states and p_z, s states separately, we find that the stacked $E_{\text{CNL}} = 0.76$ eV for the p_z, s states, and the lateral $E_{\text{CNL}} = 0.48$ eV for the $p_{x,y}$ states, both referred to the VBM. This difference is much less than for MoS₂, and originates from the fact that MoS₂ is a d^2 compound with one occupied Mo d -like valence band in the z orientation, whereas InSe has a more of the closed shell isotropic configuration.

IV. SUMMARY

We have carried out a comprehensive calculation of the electronic structure of monolayer InSe, including its band structure, bonding, band offsets against other 2D layered semiconductors, its native defects, its substitution dopants, and its contact properties. In many ways, monolayer InSe maintains the advantages of three-dimensional (3D) bonded semiconductors with low effective-mass band-edge states, and shallow dopant sites, while it also possesses many of the advantages of 2D semiconductors such as the ability to form heterostructures of different band gaps, without being subject to the constraints of lattice matching that would hold in normal 3D semiconductors. Thus it is very suitable for electronic devices such as tunnel FETs.

ACKNOWLEDGMENT

This work is supported by the EPSRC grants EP/K016663/1 and EP/P005152/1.

- [1] F. Schwierz, *Nanoscale* **7**, 8261 (2015).
- [2] K. F. Mak, C. Lee, J. Hone, J. Shan, and T. F. Heinz, *Phys. Rev. Lett.* **105**, 136805 (2010).
- [3] X. Cui, G. H. Lee, Y. D. Kim, G. Arefe, P. Y. Huang, C. H. Lee, D. A. Chenet, X. Zhang, L. Wang, F. Ye, F. Pizzocchero, B. S. Jessen, K. Watanabe, T. Taniguchi, D. A. Muller, T. Low, P. Kim, and J. Hone, *Nat. Nanotechnol.* **10**, 534 (2015).
- [4] C. Gong, H. J. Zhang, W. H. Wang, L. Colombo, R. M. Wallace, and K. J. Cho, *Appl. Phys. Lett.* **103**, 053513 (2013); **107**, 139904 (2015).
- [5] F. A. Rasmussen and K. S. Thygesen, *J. Phys. Chem. C* **119**, 13169 (2015).
- [6] H. Liu, A. T. Neal, Z. Zhu, Z. Luo, X. F. Xu, D. Tomanek, and P. D. Ye, *ACS Nano* **8**, 4033 (2014); A. Castellanos-Gomez, *J. Phys. Chem. Lett.* **6**, 4280 (2015).
- [7] Y. Guo and J. Robertson, *Sci. Rep.* **5**, 14165 (2015).
- [8] S. D. Lei, L. H. Ge, S. Najmaei, A. George, R. Kappera, J. Lou, M. Chhowalla, H. Yamaguchi, G. Gupta, R. Vajtai, A. D. Mohite, and P. M. Ajayan, *ACS Nano* **8**, 1263 (2015); W. Feng, W. Zheng, W. W. Cao, and P. A. Hu, *Adv. Mater.* **26**, 6587 (2014).
- [9] S. Sucharitakul, N. J. Goble, U. R. Kumar, R. Sankar, Z. A. Bogorad, F. C. Chou, Y. T. Chen, and X. P. A. Gao, *Nano Lett.* **15**, 3815 (2015).
- [10] D. A. Bandurin, A. V. Tyurnina, G. L. Yu, A. Mishchenko, V. Zolyomi, S. V. Morozov, R. K. Kumar, R. V. Gorbachev, Z. R. Kudrynskiy, S. Pezzini, Z. D. Kovalyuk, U. Zeitler, K. S. Novoselov, A. Patanè, L. Eaves, I. V. Grigorieva, V. I. Fal'ko, A. K. Geim, and Y. Cao, *Nat. Nano* **12**, 223 (2016).
- [11] C. Sun, H. Xiang, and B. Xu, *Appl. Phys. Express* **9**, 035203 (2016).
- [12] T. N. Theis and P. M. Solomon, *Science* **327**, 1600 (2010); A. M. Ionescu and H. Riel, *Nature (London)* **479**, 329 (2011); H. Lu and A. Seabaugh, *IEEE J. Electron. Devices* **2**, 44 (2014).
- [13] J. S. Liu, M. B. Clavel, R. Pandey, S. Datta, M. Meeker, G. A. Khodaparast, and M. K. Hudait, *J. Appl. Phys.* **119**, 244308 (2015).
- [14] S. Das, A. Prakash, R. Salazar, and J. Appenzeller, *ACS Nano* **8**, 1681 (2014).
- [15] A. Allain, J. H. Kang, K. Banerjee, and A. Kis, *Nat. Mater.* **14**, 1195 (2015).
- [16] S. J. Clark, M. D. Segall, C. J. Pickard, P. J. Hasnip, M. J. Probert, K. Refson, and M. C. Payne, *Z. Kristallogr.* **220**, 567 (2005).
- [17] S. Grimme, *J. Comput. Chem.* **27**, 1787 (2006).
- [18] S. J. Clark and J. Robertson, *Phys. Rev. B* **82**, 085208 (2010).
- [19] D. Liu, Y. Guo, L. Fang, and J. Robertson, *Appl. Phys. Lett.* **103**, 183113 (2013).
- [20] J. K. Ellis, M. J. Lucero, and G. E. Scuseria, *Appl. Phys. Lett.* **99**, 261908 (2011).
- [21] Y. Guo, D. Liu, and J. Robertson, *Appl. Phys. Lett.* **106**, 173106 (2015).

- [22] S. Lany and A. Zunger, *Phys. Rev. B* **78**, 235104 (2008).
- [23] S. Andres-Penares, A. Cros, J. P. Martinez-Pastor, and J. F. Sanchez-Royo, *Nanotechnology* **28**, 176701 (2017).
- [24] R. V. Gorbachev, *Presented at International Workshop on Novel Materials* (Kirchberg, Austria, 2017).
- [25] M. Schluter, *Nuovo Cimento B* **13**, 313 (1973).
- [26] G. Ferlat, H. Xu, V. Timoshevskii, and X. Blase, *Phys. Rev. B* **66**, 085210 (2002); V. N. Brudnyi, S. Y. Sarkisov, and A. V. Kosobutsky, *Semicond. Sci. Tech.* **30**, 115019 (2015).
- [27] M. Schluter, J. Camassel, S. Kohn, J. P. Voitchovsky, Y. R. Shen, and M. L. Cohen, *Phys. Rev. B* **13**, 3534 (1976).
- [28] J. Robertson, *J. Phys. C Solid State* **12**, 4777 (1979); **12**, 4753 (1979).
- [29] V. Zolyomi, N. D. Drummond, and V. I. Fal'ko, *Phys. Rev. B* **87**, 195403 (2013); S. J. Magorrian, V. Zolyomi, and V. L. Falko, *ibid.* **94**, 245431 (2016).
- [30] L. Debbichi, O. Eriksson, and S. Lebegue, *J. Phys. Chem. Lett.* **6**, 3098 (2015).
- [31] D. V. Rybkovskiy, A. V. Osadchy, and E. D. Obratsova, *Phys. Rev. B* **90**, 235302 (2014); D. Wickramaratne, F. Zahid, and R. K. Lake, *J. Appl. Phys.* **118**, 075101 (2015).
- [32] V. Zolyomi, N. D. Drummond, and V. I. Fal'ko, *Phys. Rev. B* **89**, 205416 (2014).
- [33] H. P. Komsa and A. V. Krasheninnikov, *Phys. Rev. B* **86**, 241201 (2012).
- [34] H. L. Zhang and R. G. Hennig, *Chem. Mats.* **25**, 3232 (2013).
- [35] D. Y. Qiu, F. H. daJornada, and S. G. Louie, *Phys. Rev. Lett.* **111**, 216805 (2013).
- [36] G. W. Mudd, A. Patane, Z. R. Kudrynskiy, M. W. Fay, O. Makarovskiy, L. Eaves, Z. D. Kovalyuk, V. Zolyomi, and V. Falko, *Appl. Phys. Lett.* **105**, 221909 (2014).
- [37] C. Ferrer-Roca, A. Segura, M. V. Andrés, J. Pellicer, and V. Muñoz, *Phys. Rev. B* **55**, 6981 (1997).
- [38] J. F. Sanchez-Royo, G. Munoz-Matutano, M. Brotons-Gisbert, J. P. Martinez-Pastor, A. Segura, A. Cantarero, R. Mata, J. Canet-Ferrer, G. Tobias, E. Canadell, J. Marques-Hueso, and B. D. Gerardot, *Nano Res.* **7**, 1556 (2014).
- [39] G. Ottaviani, C. Canali, F. Nava, P. Schmid, E. Mooser, R. Minder, and I. Zschokke, *Solid State Commun.* **14**, 933 (1974); N. Kuroda and Y. Nishina, *Physica B* **105**, 30 (1981).
- [40] T. M. Henderson, J. Paier, and G. E. Scuseria, *Phys. Stat. Solidi B* **248**, 767 (2011).
- [41] Y. Hinuma, A. Gruneis, G. Kresse, and F. Oba, *Phys. Rev. B* **90**, 155405 (2014).
- [42] W. Chen and A. Pasquarello, *Phys. Rev. B* **86**, 035134 (2012).
- [43] F. Oba, A. Togo, I. Tanaka, J. Paier, and G. Kresse, *Phys. Rev. B* **77**, 245202 (2008).
- [44] M. A. L. Marques, J. Vidal, M. J. T. Oliveira, L. Reining, and S. Botti, *Phys. Rev. B* **83**, 035119 (2011).
- [45] Y. Guo and J. Robertson, *Appl. Phys. Lett.* **108**, 233104 (2016).
- [46] Y. Huang, E. Sutter, J. T. Sadowski, M. Cotlet, O. L. A. Monti, D. A. Rucke, M. R. Neupane, D. Wickramaratne, R. K. Lake, B. A. Parkinson, and P. Sutter, *ACS Nano* **8**, 10743 (2014).
- [47] Y. Kumugai, L. A. Burton, A. Walsh, and F. Oba, *Phys. Rev. Appl.* **6**, 014009 (2016).
- [48] J. Y. Noh, H. Kim, and Y. S. Kim, *Phys. Rev. B* **89**, 205417 (2014).
- [49] W. Zhou, X. Zou, S. Najmaei, Z. Liu, Y. Shi, J. Kong, J. Lou, P. M. Ajayan, B. I. Yakobson, and J. C. Idrobo, *Nano Lett.* **13**, 2615 (2013).
- [50] J. Dabrowski and M. Scheffler, *Phys. Rev. B* **40**, 10391 (1989).
- [51] D. J. Chadi and K. J. Chang, *Phys. Rev. B* **39**, 10063 (1989).
- [52] N. F. Mott, *Adv. Phys.* **16**, 49 (1967); J. Robertson, *Philos. Mag.* **51**, 183 (1985).
- [53] K. Dolui, I. Rungger, C. Das Pemmaraju, and S. Sanvito, *Phys. Rev. B* **88**, 075420 (2013).
- [54] R. T. Tung, *Appl. Phys. Rev.* **1**, 011304 (2014).
- [55] J. Tersoff, *Phys. Rev. Lett.* **52**, 465 (1984).
- [56] W. Monch, *Phys. Rev. Lett.* **58**, 1260 (1987); *Surf. Sci.* **299**, 928 (1994).
- [57] J. Robertson, *J. Vac. Sci. Technol. B* **18**, 1785 (2000); **31**, 050821 (2013).
- [58] C. Gong, L. Colombo, R. M. Wallace, and K. J. Cho, *Nano Lett.* **14**, 1714 (2014).
- [59] J. H. Kang, W. Liu, D. Sarkar, D. Jena, and K. Banerjee, *Phys. Rev. X* **4**, 031005 (2014).
- [60] Y. Guo, D. M. Liu, and J. Robertson, *ACS Appl. Mater. Inter.* **7**, 25709 (2015).
- [61] H. B. Michaelson, *J. Appl. Phys.* **48**, 4729 (1977).
- [62] S. Kurtin and C. A. Mead, *J. Phys. Chem. Solids* **30**, 2007 (1969).
- [63] M. Schluter, *Phys. Rev. B* **17**, 5044 (1978).
- [64] S. McDonnell, R. Addou, C. Buie, R. M. Wallace, and C. L. Hinkle, *ACS Nano* **8**, 2880 (2014).
- [65] G. J. Hughes, A. Mckinley, R. H. Williams, and I. T. McGovern, *J. Phys. C: Solid State* **15**, L159 (1982).